A Dual- Linearly polarized Ku/K Band Reflectarray for Broadcast and Fixed Satellite Services

Vidhyashree Sathyanarayanan, Kavitha Narayanasamy

JOURNAL OF HIGH-FREQUENCY COMMUNICATION TECHNOLOGIES
Vol. 02 (02) (2024), pp.153-166 ***e-ISSN:2836-9009***
https://doi.org/10.58399/BCDJ534

A Dual- Linearly polarized Ku/K Band Reflectarray for Broadcast and Fixed Satellite Services

Vidhyashree S[1*], **Kavitha Narayanasamy**[2]

[1] Department of Electronics and Communication Engineering, College of Engineering, Guindy, Anna University, Chennai-600025, Tamil Nadu, India *E-mail address: vidhyashree201@gmail.com*
[2]Department of Electronics and Communication Engineering, Easwari Engineering College, Ramapuram. Chennai, India *E-mail address: kavitha9980@gmail.com*

Abstract

A distinct single-layer reflectarray (RA) featuring dual polarization and dual-band capabilities has been developed, integrating distinct control mechanisms for each frequency band. The downlink element in the Ku-band employs a vertical slot embedded with semi-circular rings, featuring 841 elements, and is complemented by two delay lines attached to the outer ring to ensure orthogonal polarization. The uplink containing 841 elements was formed by 90° rotation of downlink element in order to avoid mutual coupling effect. The application of the degree of freedom (DOF) enabled the attainment of phase ranges of 720° and 840° within the unit cell for both the frequency bands. 1682 elements were etched over the Taconic TLx-09 substrate of 0.8mm thickness with aperture size of $16.5\lambda_0 \times 16.5\lambda_0$ mm was developed, simulated, and experimentally verified for Ku and K band applications. The centre-fed reflectarray upon construction exhibited a measured gain of 26.5dBi and 25.7 dBi and 1dB gain bandwidth of 26.4% for Ku band and 11.7% for K band respectively. The proposed reflectarray also demonstrated a maximum aperture efficiency of 30.4% at 12.8 GHz and 19% at 23 GHz. Thus, the proposed dual-polarization reflectarray covered the downlink frequencies for the broadcasting satellite communication services like DTH connectivity and uplink frequencies for earth exploration satellite services like high-speed internet access and video conferencing.

Keywords: *Reflectarray, Orthogonal polarization, Single layer, Dual-band, Satellite Communication Services*

1. Introduction

Earth exploration satellite services (EESS) is intended for the analysis of environmental conditions and forecast of hazardous weather conditions like drought, heavy rain, stratospheric ozone depletion arising as the result of global warming. EESS is inevitable in environmental monitoring for the analysis of the quality of environment, meteorology and cartography. Reflectarray antennas (RAs), which combine key features of reflectors and phased arrays, have emerged as the optimal solution for satellite communication Dahri et al. (2017). RA, owing to its salient characteristics like low profile, easily deployable, planar and structure simplicity has been identified as a proactive candidate for applications like remote sensing, deep space telemetry and TV signal broadcasting Narayanasamy et al. (2020). Different methodologies employed in the design of dual-band RAs include the utilization of active components such as PIN diodes Suresh (2023) and varactor diodes

[*]**Corresponding author**
Received: 18^{th}, March 2024, Revised: 08^{th} June, 2024, Accepted: 20^{th} June 2024 and available online 28^{th} June 2024

Suresh et al. (2023), as well as the incorporation of cross dipoles with fixed rings for Ku-band and circular patches with adjustable ring sizes for Ka-band Zhao et al. (2017), cross-dipole, double ring elements for X and Ku bands Pan et al. (2014) and axially symmetric dual reflectarray Yoon et al. (2014). But these designs have low polarization purity, bandwidth limitation and higher fabrication cost due to usage of stacked multi-layer. Several literature analyses have been employed for the attainment of orthogonal polarisation and to ensure polarisation purity, enough bandwidth and reduction in manufacturing expenses. Considering frequency ratio as the vital aspect for dual-band, literature is focussed on frequency bands, namely, X/ Ku bands and X/K bands.

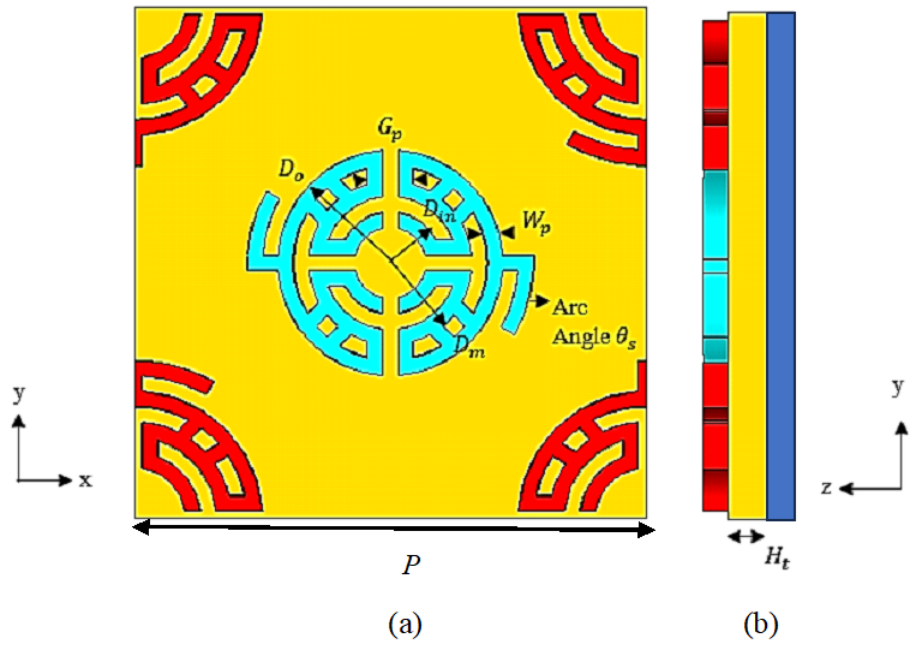

Figure 1. Design of unit cell Layout covering (10.5 GHz -14.6 GHz) (a) Front view (b) Profile view

A multi-layer RA containing 15616 elements designed contains square patch operating for both polarizations Zornoza and Encinar (2004). These elements provide a gain of 36dBi and 33dBi in both polarizations at 13.5 GHz. Furthermore, FSS backed 40mm Ku band elements are positioned above the conventional X band RA of 162mm for the improvement of the isolation between the elements. The unit cells operate in closer frequencies compared to other dual-band RA through, use of FSS. The Ku and X band provide peak gain of 24.68dB and 24.75dB along with 44% and 40% efficiency respectively. However, the stacking of layers increases complexity. The unit cells operate in closer frequencies compared to other dual-band RA with the use of the FSS property Derafshi et al. (2016) & Abdollahvand et al. (2020b). However, with the use of stacked multi-layer RA, fabrication cost is the main short-coming. Hence, as a low-cost measure, multi-frequency operation using single layer is achieved as further improvement. In Aryanian et al. (2019), individual elements are arranged in integrated fashion with additional air gap for achievement of polarization purity for the realization of dual band dual polarization operation.

Table 1. Proposed Parameters for Ku band Unit Cell

Parameters	θ_s	D_{in}	D_m	D_o	G_p	H_t	W_p	P
Value (mm)	30°	(0.7-1.7)	(1.3-2.6)	(1.9-3.2)	0.3	0.8	0.3	10

The uplink and downlink elements are designed at centre frequencies of 14.25 GHz and 11.3 GHz to provide a gain of 30.6dBi and 27.1dBi respectively. However, mutual coupling effect is prominent in this RA structure. The slot type metal phoenix elements use multi-parameter sweeping for the achievement of the desired phase range Deng et al. (2017). The metal only RA provides gain of

29.1 dBi at 10 GHz and 32.6 dBi at 15 GHz. A 5 mm air gap has been introduced for increase in bandwidth, which improves RA performance. Two sets of miniaturized fractal patches were designed for operation at frequencies of 28/32 GHz, for 5G cellular applications enabling dual-frequency operation 25.7 dBi and 28.5 dBi gain were achieved at lower and higher frequencies along with 29% and 38% aperture efficiencies respectively with the use of 225 elements. Although Deng et al. (2017) and Costanzo et al. (2020) provide polarization purity, mutual coupling effect was prominent in this RA structure. Karimipour and Aryanian (2022) designed a broadband element using the polarization conversion technique (PCT). The anisotropic meta surface containing 841 "I" shaped metal patch of 290 cm × 290 cm provided 1dB gain of 17.41% and 30.3% respectively. But, the PCT along with additional air gap increased complexity.

Table 2. Proposed Parameters for K band Unit Cell

Parameters	θ_s	U_{in}	U_m	U_o	M_p	H_1	W_p	P
Value (mm)	30°	(0.7-1.7)	(1.3-2.6)	(1.9-3.2)	0.3	0.8	0.3	10

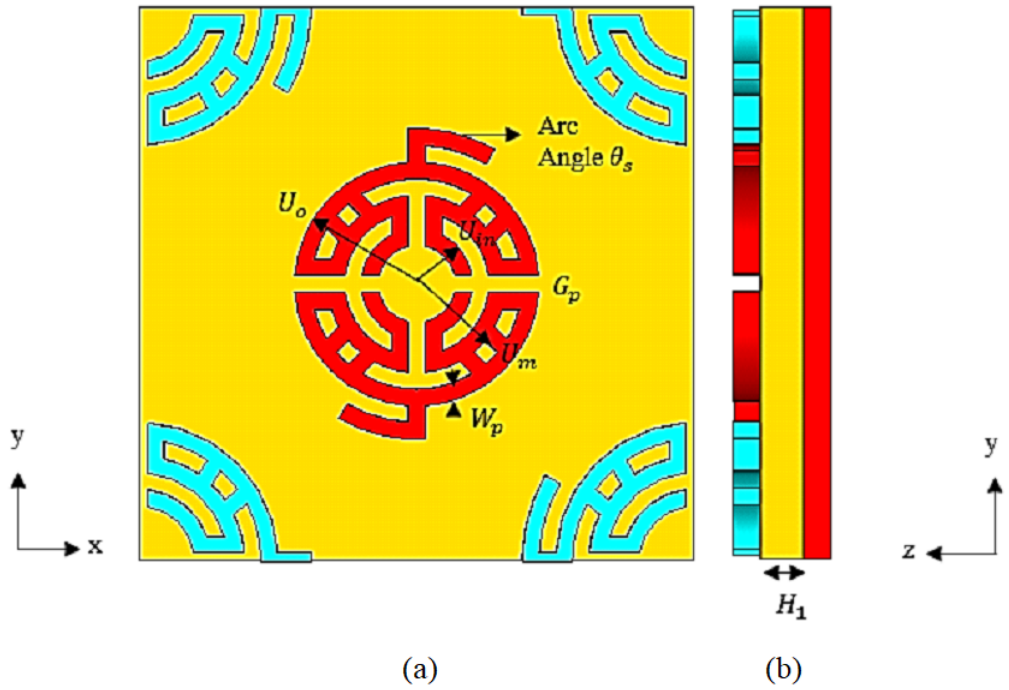

Figure 2. Design of unit cell Layout covering (21.5GHz-24.5 GHz) (a) Front view (b) Profile view-Red-K band unit cell, Blue- Ku band unit cell, Yellow-substrate, Dark Blue-Ground

A novel single-layer design Abdollahvand et al. (2020a) & Malfajani and Atlasbaf (2014), comprising cross dipoles with four modified truncated rings optimized for 30 GHz, along with cross-shaped loops tailored for 20 GHz operation was developed for the elimination of complexity. Dual-band dual polarization has been achieved through independent adjustment of individual elements. With 1296 elements spanning 18×18 cm, the system achieves gains of approximately 30 dBi and 33 dBi at frequencies of 20 GHz and 30 GHz respectively. The inference from the literature studies is that there is a strong requirement of dual polarized dual-band RA for Ku/K band frequencies. The subsequent sections of this paper are structured as follows. Section 2 provides a description of the evolution, characterization, and details of parametric analysis of integrated elements for dual frequencies, with the discussion of the equivalent circuit modelling along with surface current distribution. Section 3 explains the proposed dual-band reflectarray with dual polarization characteristics along with reflection phase distribution and measurement setup. Section 4 provides details relating to the experimental results such as radiation pattern, gain, aperture efficiency, cross-polarization values, performance comparison with existing work and conclusion.

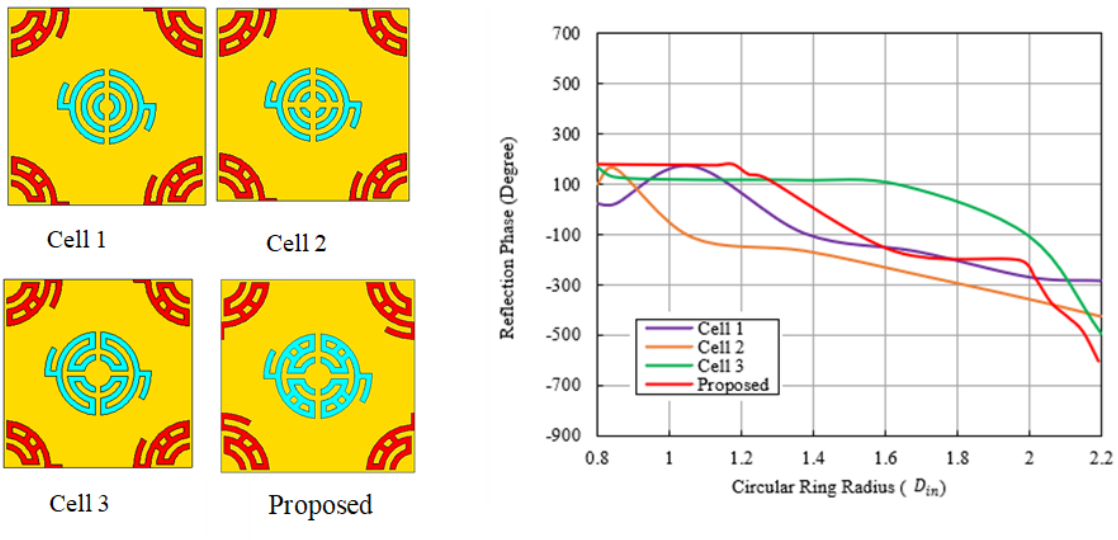

Figure 3. Construction Steps of Ku band unit cell

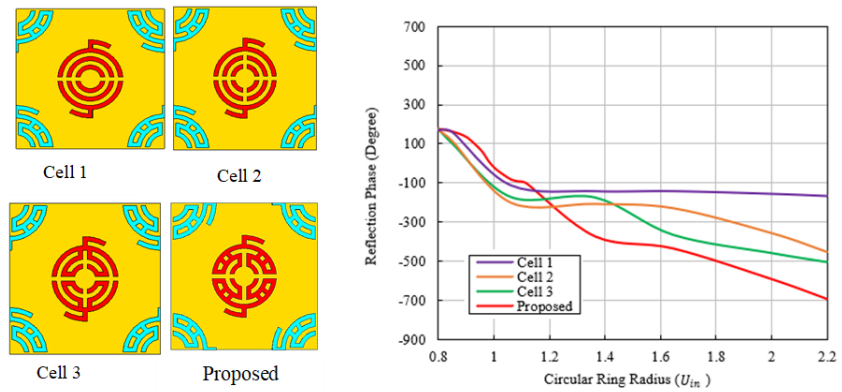

Figure 4. Construction Steps of K band unit cell

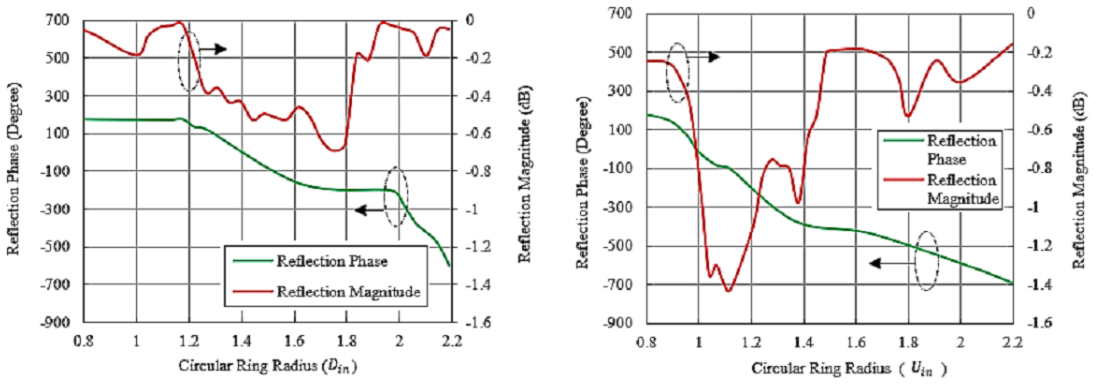

(a) (b)

Figure 5. The reflection properties of (a) (10.5 GHz-14.6 GHz) band unit cell (b) (21.5GHz-24.5 GHz) band unit cell

2. Dual Polarized Unit Cell Analysis

2.1. Integrated Unit Cell Characterization

This paper emphasizes the design of a wideband unit cell with dual-linear polarization capabilities, aiming at the achievement of optimal performance in both polarization modes. Conduct of theoretical analyses, helped the desired polarization characteristics through the utilization of a vertical slot for horizontal polarization and vice versa. The slot structure was utilized in the circular loop for the implementation of polarization, thereby forming a pair of semi-circular loops Suresh et al. (2022). The phase delay lines, situated at the outer ring with opposite-facing configurations, operated at 12.8 GHz for the downlink element. The selection of unit cell dimensions had influence primarily from the slots within the elements and the phase delay line, representing two deterministic factors. The novel unit cell element, incorporating incremental phase variation,

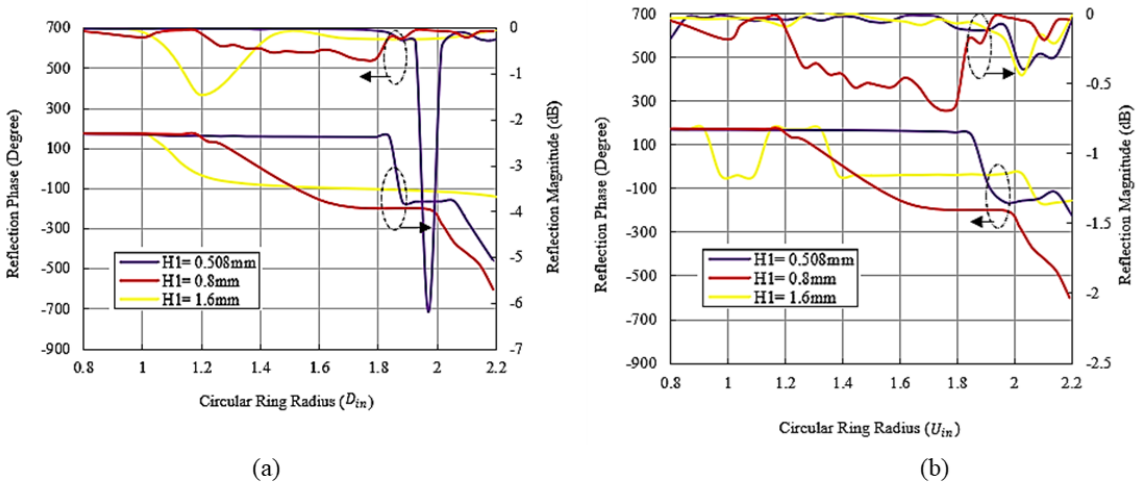

Figure 6. Optimal correlation between reflection phase and varies size of circular Ring with different substrate height (a) (10.5GHz-14.6 GHz) band unit cell (b) (21.5 GHz-24.5 GHz) band unit cell

provided freedom of large degree, facilitating the attainment of reflection phases exceeding 360° and minimizing cross-polarization effects. A metal patch was positioned on a single layer dielectric substrate whose thickness is 0.8mm and dielectric constant ϵ_r is 2.55. A preliminary depiction of the pair of semi-circular loops featuring a vertical slot and an attached phase delay line at the outer end was created shown in Fig 1. The proposed single-layer structure was characterized by unit cell dimensions of 10 mm × 10 mm. These two symmetrical arc-shaped sections extending from the centre point of the circular loop, thereby constituting the phase delay line. Consequently, the phase delay line went through rotation by an arc angle θ_s, θ representing the opening angle subtended by the two arc-shaped sections. Degrees of freedom with four independent parameters such as D_{in}, G_p, W_p and θ_s were utilized for the achievement of the phase variation.

The complete Ku band element was positioned at the centre while K element at the margins were positioned with element size of 10mm as shown in Fig. 2. Choice of an inter-element separation of 10mm as the unit cell size ensured separation between elements staying below one free space wavelength. Single-layer dual-polarized unit cells were designed on a Taconic TLX-09 substrate with a height of 0.8mm, a ϵ_r of 2.55, and a loss tangent (tan δ) of 0.015. The integrated elements periodicity for Ku band was fixed as $0.42\lambda_0$ and $0.76\lambda_0$ for K band having element size fixed as 10 mm. Values for spacing and width established were $G_p = 0.3$ mm for accounting for fabrication tolerances in the PCB process. Analysis of element design employing Floquet ports and periodic boundary conditions were conducted using CST software. Table 1 and 2 provide summaries of the finalized parameters for the Ku/K-band unit cell elements respectively.

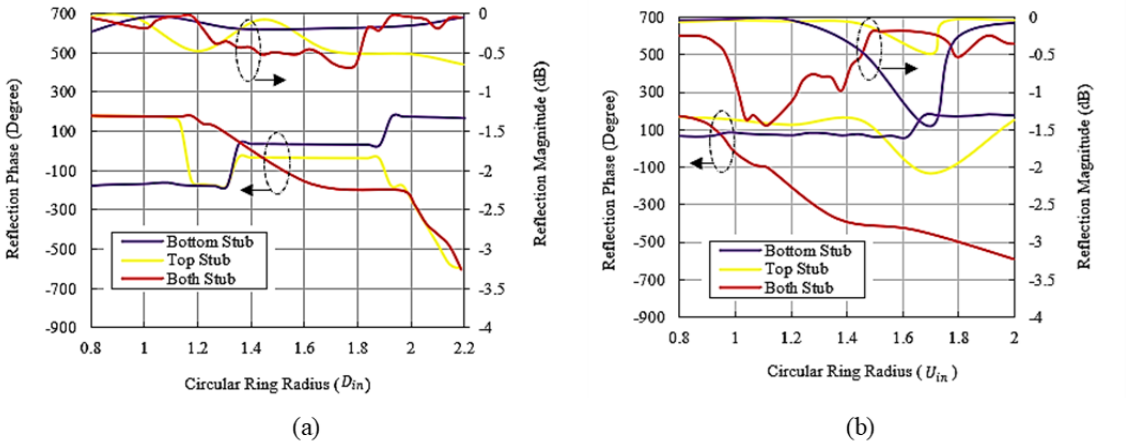

Figure 7. Optimal correlation between reflection phase and varies sizes of circular Ring with different substrate height (a) (10.5GHz-14.6 GHz) band unit cell (b) (21.5 GHz-24.5 GHz) band unit cell

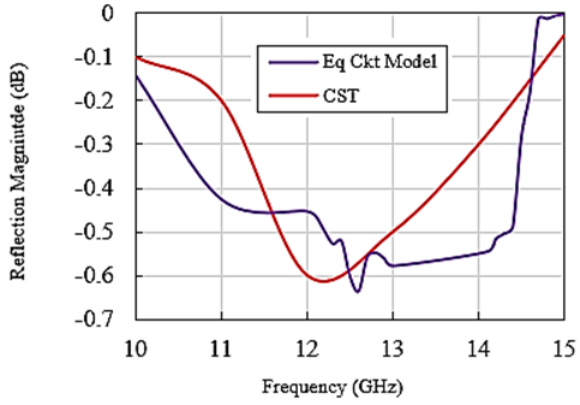

Figure 8. Reflection magnitude of equivalent circuit for Ku band frequencies using CST and ADS software model

2.2. Evolution of Unit cell

The designed Ku-band unit cell features three circular loops created by the vertical slot positioned relative to the centre of each circular loop, as depicted in Fig. 3, along with a horizontal slot for the K-band, illustrated in Fig. 4. In order to preserve symmetry among the elements, two delay lines were affixed to the outer circular structure, positioned with 30° arc length on opposite faces of the main circular loop. The development of the unit cell1 was derived from the concentric circular ring structure, resulting in a phase range of 383°. A horizontal capacitive slot was introduced within the inner and middle rings of cell 2 for further enhancement of resonance, resulting in a phase range of 450°. Thickness with a gap within the circular loop structures were meticulously selected to ensure the induction of coupling effects within the unit cell 3. Inductive stubs were introduced between the outer and middle circular rings as shown in Cell 3. This modification has resulted in a unit cell bandwidth exceeding 50%, accompanied by a phase range of 640° for enhancement of the bandwidth of the unit cell. Inductive stubs have been incorporated between the inner and middle circular rings for enhancement of the unit cell's bandwidth. This adjustment led to a unit cell bandwidth surpassing 50% coupled with a phase range of 640°. In conclusion, enhancement of linearity and a smoother phase slope is achieved by connecting the middle and inner circular loops, resulting in a bandwidth exceeding 60%, a phase range of 720°, and a reflection magnitude below 0.8dB.The proposed configuration has provided demonstration

of broader resonating behaviour at 12.8 GHz, depicted in Fig. 5(a). Likewise, the re-radiating elements adopted a comparable approach for the K-band, yielding a phase range of 840°, shown in Fig. 5(b), with reflection magnitude less than 1.6dB at 23 GHz indicating the suitability of this element for broadband performance.

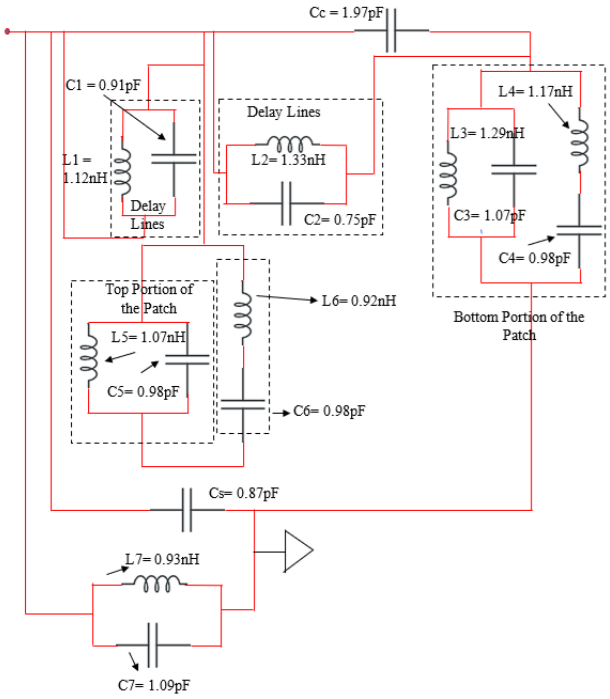

Figure 9. Modelling the Equivalent Circuit for Ku band unit cell

2.2.1. Parametric Analysis

A parametric investigation was conducted on Ku/K-band re-radiating elements for evaluation of the optimal properties of the unit cell with variations in the thickness and inductive stubs of the main patch while considering Din as the degrees of freedom. Available literature indicates the influence of substrate height on both the phase range and slope of the phase curves. A thinner substrate resulted in a broader phase range and a steeper slope, whereas a thicker substrate narrowed the phase range with attenuation of the slope. Initially, for Ku band, with $H_1 = 0.50$mm, a very narrower steep magnitude was achieved while for the height $H_1 = 1.6$mm, the phase range achieved was 350°. Hence, as a trade-off between wider phase range and slope, $H_1 = 0.80$mm was chosen as an optimum value. The unit cell behaviour satisfied the requirements of gradual slope shifting and a larger phase range for $H_1 = 0.80$mm and permittivity values of the substrate $\epsilon_r = 2.55$. Figure 6(a) and (b) show the finalized optimum values for K-band. Further, the inductive stubs are investigated to determine the unit cell characterization. Studying the inductive stub behaviour, a steeper slope with a smaller bandwidth was obtained in both the Ku and K band frequencies utilising only the top or bottom half of the stub. Smoother phase slope and a lower sensitivity value are only possible when both top and bottom inductive stubs were used. Hence both stubs were utilized for unit cell characterization as shown in Fig. 7(a) and (b).

2.2.2. Analysis using Equivalent Circuit and Surface Current Distribution

The integrated elements are assessed for their dual-band behaviour through an equivalent circuit modelling approach. The two semi-circular loop is designed as two portions mainly left and right part connected by coupling capacitor. The entire circuit was considered as parallel plate capacitance (C_L, L_L) and (C_R, L_R) connected by coupling capacitor C_C.The semi-circular ring

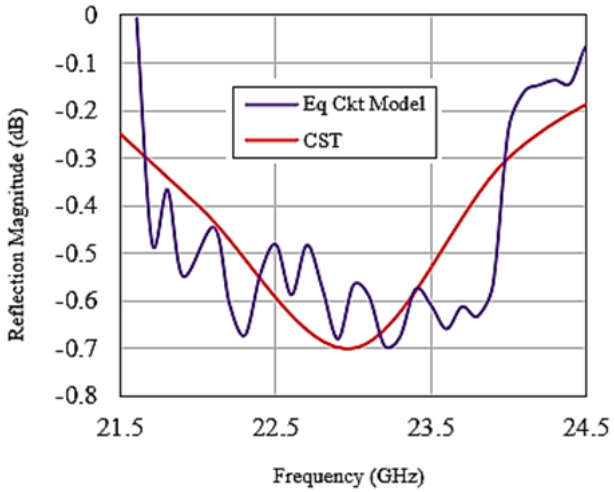

Figure 10. Reflection magnitude of equivalent circuit for K band frequencies using CST and ADS software model

contains the outer circular ring (C_L, L_L connected in parallel fashion with the coupling capacitor to the right portion of the semi-circular ring as $(C_u, L_u) \parallel C_c \parallel (C_l, L_l)$. Figure 8 illustrates the graph derived from the simulation model, revealing a close alignment between the reflection magnitude values obtained from the equivalent circuit for the Ku band. The equivalent circuit was represented in parallel LC configuration, with minimal ohmic losses neglected Hum and Du (2017), as illustrated in Fig. 9 for the Ku band. Figure 10 is the graph obtained from CST simulation, demonstrating a close concordance with the reflection magnitude values derived from the equivalent circuit. By tuning the equivalent circuit parameters, the resonance is achieved at the centre frequencies at both bands and the values achieved through CST and equivalent circuit modelling are in close match with each other as shown in Fig. 11. Additionally, the profound behaviour of the re-radiating elements was examined through the analysis of surface current electric fields. At 12.8 GHz the induced electric field polarized in the X-direction maximum at 144 A/m was shifted from the outermost ring towards the innermost portion at resonant frequencies. This demonstrates the effectiveness of the coupled semi-circular ring structure, as illustrated in Fig. 12(a). Likewise for K band at 23 GHz, the E field surface current in the delay lines is in opposite direction hence getting cancelled with each other as shown in Fig. 12 (b). This delay line current distribution contributes for reduced cross-polarization of -27dB and -31dB for Ku and K band. The equation representing the left portion of the patch, including the delay lines, is expressed as Equ. 1

$$Z_{lp} = \frac{j\omega L1}{1-\omega^2 L1C1} + \frac{j\omega L2}{1-\omega^2 L2C2} + \frac{1-\omega^2 L3C3}{j\omega C3} \tag{1}$$

The equation representing the right portion of the patch, including the delay lines, is expressed as Equ. 2

$$Z_{rp} = \frac{-\omega^2 L4C4}{j\omega C4 + j\omega L4} + \frac{-\omega^2 L5C5}{j\omega C5 + j\omega L5} + \frac{1}{j\omega C6} + j\omega L6 \tag{2}$$

The equation describing the upper section of the unit cell, incorporating delay lines is expressed as Equ. 3,

$$Z_{tp} = \frac{-\omega^2 L1C1}{j\omega C1 + j\omega L1} + \frac{-\omega^2 L2C2}{j\omega C2 + j\omega L2} + \frac{1}{j\omega C3} + j\omega L3 \tag{3}$$

The Equ.4 describing the lower section of the re-radiating element, incorporating delay lines is,

$$Z_{bp} = \frac{-\omega^2 L4C4}{j\omega C4 + j\omega L4} + \frac{-\omega^2 L5C5}{j\omega C5 + j\omega L5} + \frac{1}{j\omega C6} + j\omega L6 \tag{4}$$

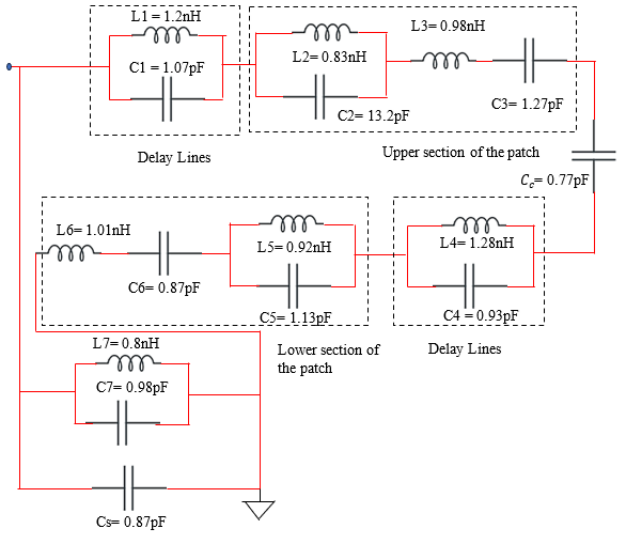

Figure 11. Development of an equivalent circuit model for the Ku-band unit cell

3. Dual-Band RA Design with Dual Polarization

A dual-band reflectarray (33 cm) consisting of 1682 elements was developed on Taconic TLX-09 substrate for operation at K-band (23.5 GHz) and Ku-band (14.5 GHz), utilizing element compensation. The phase compensation to be provided by 29×29 dual-band elements to compensate the spatial phase delay is provided by Equ. 5 Narayanasamy et al. (2021).

$$\Phi_{mn(r)} = k_0(d_i - (x_i cos\Phi_0 + y_i sin\Phi_0) \times sin\theta_0) \tag{5}$$

The Ku-band elements were arranged concentrically, with the center element and source coinciding. In contrast, for the K-band, the central element was offset by 5mm in right hand side direction relative to the source. A total of 210 elements were positioned within the first division of the reflectarray board for the Ku band elemetns, considering their symmetric nature. Subsequently, these elements were mirrored along the X-axis, followed by mirroring the top half portion along the Y-axis for completion of the reflectarray elements. In the case of elements covering (21.5GHz-24.5 GHz), a specialized arrangement was implemented. To start with, 105 elements were mirrored along the X-axis for obtaining the right-side division of the reflectarray elements. Then, a second mirroring process was applied to mirror the 1/4th portion of right-side elements to the lower 3rd side division. Similarly, the values of the left-side portion were mirrored down to the last quadrant. These processes are illustrated in Fig. 13 (a) & (b). The integration of elements with dual polarization characteristics provided enhancement of the phase alignment at resonant frequencies. The reflectarray antenna is fed using standard Ku/K-band pyramidal horns, featuring a flare length of 54mm, integrated with a waveguide of an aperture size of 20×11mm. In the H-plane, it achieves a peak gain of 17.4dBi at 12.8 GHz. Similarly, for the K-band, a standard pyramidal horn with a flare length of 20.5mm was connected to a waveguide of the same aperture size. This provided a gain of 16.75dBi at 23 GHz in the E-plane. Consequently, the optimal K/Ka-band pyramidal horn, serving as the source, was positioned in front of the reflectarray antenna at a distance of 26.4cm, considering an F/D ratio of 0.8 to ensure the required aperture efficiency. Thus, the fabricated prototype was tested in the anechoic chamber facility of size 7×3×3 meter integrated with Agilent N9917A handheld network analyser for measurement of radiation pattern and gain characteristics, which is illustarted in Fig.14 (a) and (b). In efficiency measurements, the primary factor influencing efficiency, particularly in the K-band, was the feed-blockage resulting from the center feed of the antenna. Other potential factors affecting efficiency included backscattering from the phase-delay lines, dissipative loss of the substrate, fabrication errors, reflection from the ground plane, and element phase errors. Utilizing low-loss substrates or employing an offset feed design can enhance antenna efficiency Narayanasamy et al. (2021).

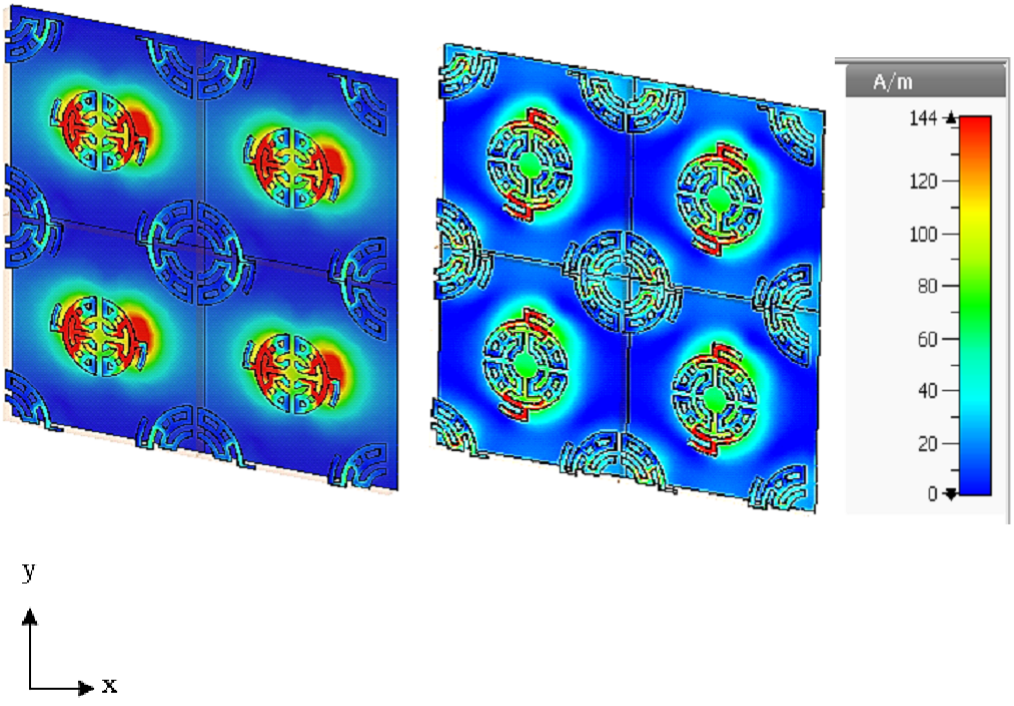

Figure 12. Current Distribution along the surface of unit cell at (a) the (10.5GHz-14.5 GHz) Band and (b) (21.5GHz-24.5 GHz) Band

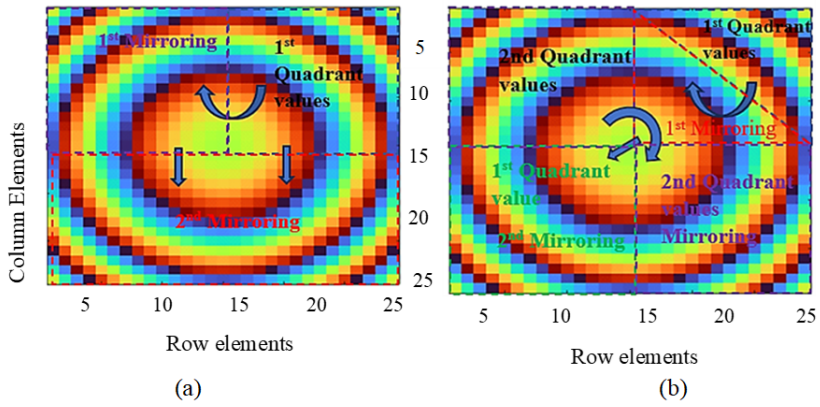

Figure 13. Reflection Phase distribution for a grid of 29×29 re-radiating elements (a) Ku Band Homo-centrically elements (b) K band counteractly placed elements

3.1. Experimental Results and Outcomes

The normalized radiation patterns of E-plane and H-plane, both measured and simulated, along with cross-polarization, are illustrated in Fig 15. Additionally, the measured gain was plotted using the radiation pattern magnitude, utilizing the Friis transmission formula. The 1-dB gain bandwidths for Ku/K-band frequencies were 26.4% and 11.9%. Peak gains achieved were 26.5 dBi and 25.7 dBi for Ku/K band, respectively. Discrepancies between measured and simulated gain arose from misalignment and fabrication errors at both frequencies. Sidelobe levels, measured along with principal planes, were -17.9 dB and -16.3 dB, with aperture efficiencies of 30.4% and 19%, respectively Dahri et al. (2020). The gain obtained seen was lower due to the special arrangement placed offset of K-band elements compared to Ku-band elements. The measured cross-polarization

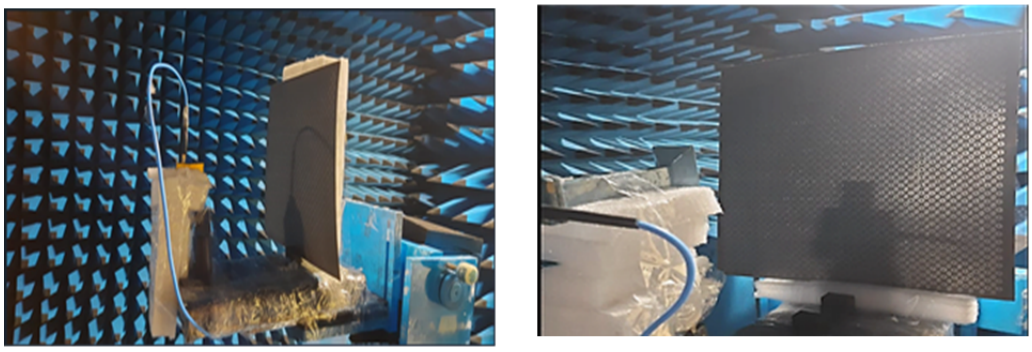

Figure 14. Arrangement for measuring the designed reflectarray with (a) Perspective View (b) Side View

values seen were -28dB and -31dB respectively.

Table 3. Performance Evaluation of the Proposed Work compared with Existing Literature

Parameters	**This work**	**(Zhao et al., 2017)**	**(Derafshi et al., 2016)**	**(Malfajani and Atlasbaf, 2014)**	**(Abdollahvand et al., 2020b)**
Centre Freq (GHz)	12.8/23	16/35	8.5/17.5	10/20	20/30
Phase Range (°)	720°/840°	>360°	360°/360°	Above 360°/360°	450°/450°
No. of Elements	1682	441 for sub-reflectarray	324	2809	1296
Independent Control over each band	Yes	Yes	Yes	No	Yes
Aperture Size (mm)	330	170	162	400	180
Gain (dBi)	26.5/25.7	28.57/24.3	24.75/24.68	30.3/36.1	28.02/31.65
1 dB Gain BW (%)	26.4/11.9	11.6% & 7.5% (3dB)	12/11	10.2/15.1	-
SLL (dB)	-17.9/-16.3	>11dB	-15	<-21.1/<-20.52	-

Table 3 provides a comparative analysis of the proposed dual-polarized reflectarray antenna used in earlier studies documented in the literature. In comparison with the other existing literature, the following results are highlighted:

1. The 1dB gain bandwidth of the proposed reflectarray for dual-band elements outperforms existing works Zhao et al. (2017), Derafshi et al. (2016), Malfajani and Atlasbaf (2014) & SathyaNarayanan et al. (2024)references, with the achievement of 26.4% and 11.9% over the frequency ranges of 10.5-14.6 GHz and 21.5-24.5 GHz, respectively.

2. In contrast to values reported in Pan et al. (2014), Yoon et al. (2014) & Zornoza and Encinar (2004), this study presents improved 3dB pencil beamwidths of 5.2° and 5.6° for Ku and K band frequencies, respectively.

3. The proposed dual-band reflectarray, leveraging dual-polarization properties, eliminates the need for element optimization due to independent control over each band.

4. Implementation of integrated elements in this work results in higher isolation between the

two bands compared to other literature papers such as Zhao et al. (2017), Derafshi et al. (2016) & Malfajani and Atlasbaf (2014).

5. The cross-polarization is less than 28dB compared to details seen in literature Zhao et al. (2017), Abdollahvand et al. (2020a)& Malfajani and Atlasbaf (2014).

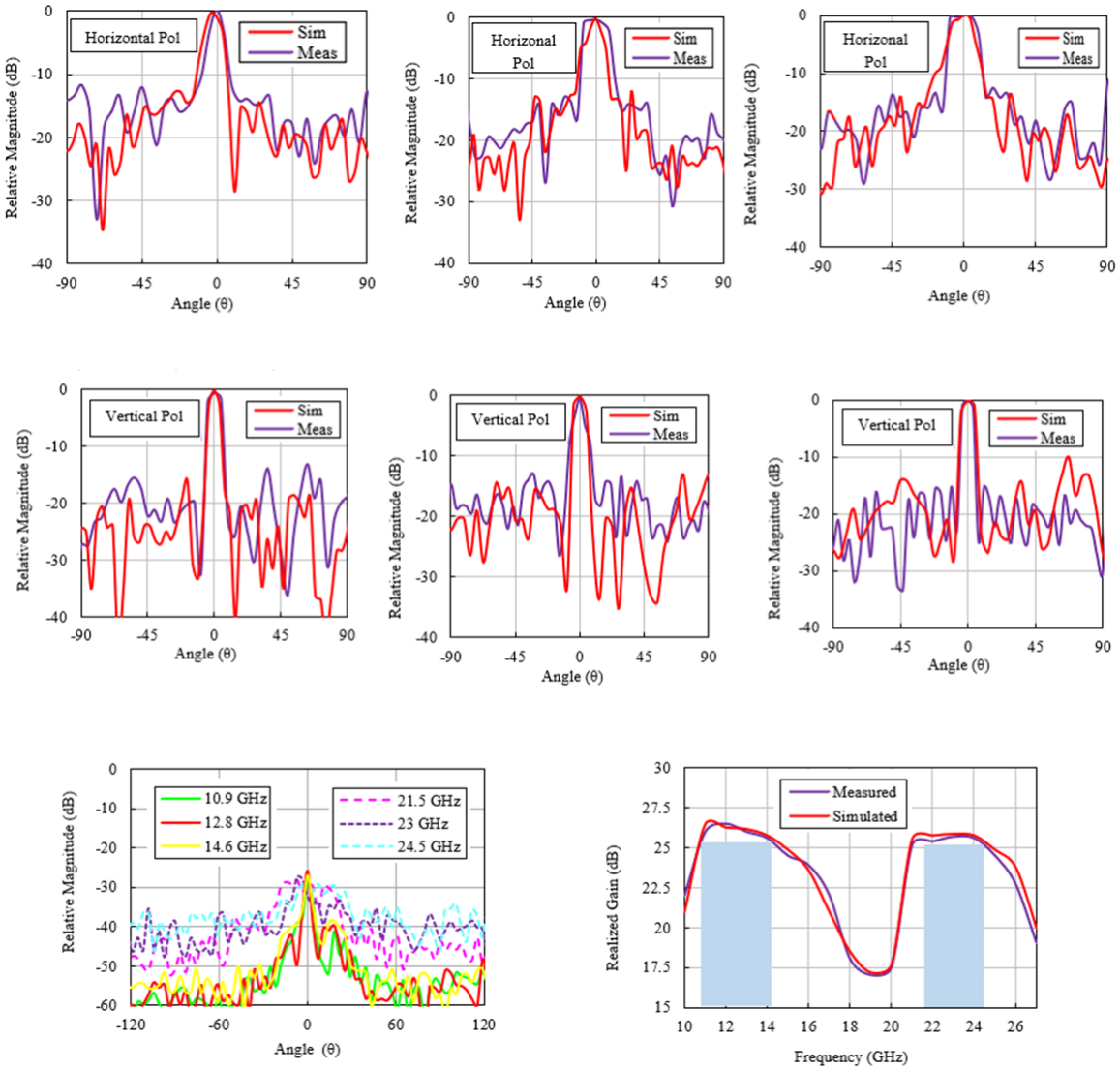

Figure 15. Simulated and measured normalized radiation patterns are obtained for various frequencies at (a) 10.9 GHz (b) 12.8 GHz (c) 14.6 GHz and (d) 21.5 GHz (e) 23 GHz (f) 24.5 GHz (g) Cross Polarization (h) Gain Plot of Dual-band

4. Conclusion

The proposed RA with wide bandwidth of 3 GHz in both uplink and downlink frequencies, along with its planar profile and high gain characteristics, positions it as an essential candidate for satellite communication services. The unit cell designed at 12.8 GHz, consisting of a pair of hemicycle rings, achieved a phase range of 720°, whereas, for the center frequency 23 GHz, the phase range extended to 840°. Both unit cells offered a 50% bandwidth. Attainment of orthogonal polarization was facilitated through coupled slot structures within the unit cell, with effective reduction in mutual coupling effects among nearby elements. The integrated 1682 elements etched

on Taconic TLX-09 substrate allows for independent control over each band and presence of identical elements minimized the mutual coupling effect between elements. The co-centric Ku band element offered a gain of 26.5dB and off-centric K band elements provides 25.7dB gain. The measured SLL values reported were -17.9dB and -16.3dB along with 1dB gain of 26.4% and 11.9% and cross polarization values were -30dB and -27dB respectively. Thus, the proposed dual-band dual polarization RA became proactive candidate for direct broadcast satellite service communications and for fixed satellite services through achievement of optimal values compared to other literature papers SathyaNarayanan et al. (2024).

Acknowledgement

The authors thank SSN College of Engineering for the support in the measurement of the antenna.

References

Abdollahvand, M; Forooraghi, K; Encinar, J. A; Atlasbaf, Z, and Martinez-De-Rioja, E. Design and fabrication of a novel single-layer ka-band reflectarray antenna. *International Journal of Microwave and Wireless Technologies*, 12, 2020a. ISSN 17590795. doi: 10.1017/S1759078719001582.

Abdollahvand, M; Forooraghi, K; Encinar, J. A; Atlasbaf, Z, and Martinez-De-Rioja, E. A 20/30 ghz reflectarray backed by fss for shared aperture ku/ka-band satellite communication antennas. *IEEE Antennas and Wireless Propagation Letters*, 19, 2020b. ISSN 15485757. doi: 10.1109/LAWP.2020.2972024.

Aryanian, I; Ahmadi, A; Rabbani, M; Hassibi, S, and Karimipour, M. Design and fabrication of a dual-polarized, dual-band reflectarray using optimal phase distribution. *Turkish Journal of Electrical Engineering and Computer Sciences*, 27, 2019. ISSN 13036203. doi: 10.3906/elk-1807-324.

Costanzo, S; Venneri, F; Borgia, A, and Massa, G. D. Dual-band dual-linear polarization reflectarray for mmwaves/5g applications. *IEEE Access*, 8, 2020. ISSN 21693536. doi: 10.1109/ACCESS.2020.2989581.

Dahri, M. H; Jamaluddin, M. H; Seman, F. C; Abbasi, M. I; Sallehuddin, N. F; Ashyap, A. Y, and Kamarudin, M. R. Aspects of efficiency enhancement in reflectarrays with analytical investigation and accurate measurement, 2020. ISSN 20799292.

Dahri, M. H; Jamaluddin, M. H; Abbasi, M. I, and Kamarudin, M. R. A review of wideband reflectarray antennas for 5g communication systems. *IEEE Access*, 5, 2017. ISSN 21693536. doi: 10.1109/ACCESS.2017.2747844.

Deng, R; Xu, S; Yang, F, and Li, M. Design of a low-cost single-layer x/ku dual-band metal-only reflectarray antenna. *IEEE Antennas and Wireless Propagation Letters*, 16, 2017. ISSN 15361225. doi: 10.1109/LAWP.2017.2698099.

Derafshi, I; Komjani, N; Ghasemi-Mizuji, E, and Mohammadirad, M. Dual-band x/ku reflectarray antenna using using a novel fss-backed unit-cell with quasi-spiral phase delay line. *Journal of Microwaves, Optoelectronics and Electromagnetic Applications*, 15, 2016. ISSN 21791074. doi: 10.1590/2179-10742016v15i3582.

Hum, S. V and Du, B. Equivalent circuit modeling for reflectarrays using floquet modal expansion. *IEEE Transactions on Antennas and Propagation*, 65, 2017. ISSN 0018926X. doi: 10.1109/TAP.2017.2657483.

Karimipour, M and Aryanian, I. High-efficiency dual-polarized broadband reflecting metasurface using continuous polarization conversion technique and element with multi degree of freedom. *Scientific Reports*, 12, 2022. ISSN 20452322. doi: 10.1038/s41598-022-11694-8.

Malfajani, R. S and Atlasbaf, Z. Design and implementation of a dual-band single layer reflectarray in x and k bands. *IEEE Transactions on Antennas and Propagation*, 62, 2014. ISSN 0018926X. doi: 10.1109/TAP.2014.2327137.

Narayanasamy, K; Mohammed, G. N. A; Savarimuthu, K; Sivasamy, R, and Kanagasabai, M. A comprehensive analysis on the state-of-the-art developments in reflectarray, transmitarray, and transmit-reflectarray antennas, 2020. ISSN 1099047X.

Narayanasamy, K; Mohammed, G. N. A; Savarimuthu, K; Sivasamy, R, and Kanagasabai, M. A novel ku/k band reflectarray antenna with reduced phase slope and phase sensitivity. *International Journal of RF and Microwave Computer-Aided Engineering*, 31, 2021. ISSN 1099047X. doi: 10.1002/mmce.22699.

Pan, Y; Zhang, Y. R, and Yu, X. A x/ku dual-band reflectarray design with cosecant squared shaped beam. *Microwave and Optical Technology Letters*, 56, 2014. ISSN 10982760. doi: 10.1002/mop.28525.

SathyaNarayanan, V; Agumbe, P; Mohammed, G. N. A, and Kanagasabai, M. A ku/k band dual linearly polarized reflectarray for earth exploration satellite services. *International Journal of Electronics*, 2024. ISSN 13623060. doi: 10.1080/00207217.2024.2302338.

Suresh, V. Optimum design of a novel electronically reconfigurable reflectarray antenna for x/ku band applications. *Journal of High-Frequency Communication Technologies*, 01:12–23, 2 2023. doi: 10.58399/DAUK9418.

Suresh, V; Mohammed, G. N. A, and Narayanasamy, K. A novel broadband reflectarray for 5g satellite communications. *International Journal of RF and Microwave Computer-Aided Engineering*, 32, 2022. ISSN 1099047X. doi: 10.1002/mmce.22972.

Suresh, V; Bhattacharjee, A, and Savarimuthu, K. Dual-layer beamscanning reflectarray antenna operating at ku-band. *Journal of High-Frequency Communication Technologies*, 01:24–34, 2 2023. doi: 10.58399/SULR8973.

Yoon, J. H; Yoon, Y. J; Lee, W. S, and So, J. H. Axially symmetric dual-reflectarray antennas. *Electronics Letters*, 50, 2014. ISSN 00135194. doi: 10.1049/el.2014.0977.

Zhao, J; Li, T; Cui, X; Zhao, X; Li, H; Hu, B; Wang, H; Zhou, Y, and Liu, Q. A low-mutual coupling dual-band dual-reflectarray antenna with the potentiality of arbitrary polarizations. *IEEE Antennas and Wireless Propagation Letters*, 16, 2017. ISSN 15361225. doi: 10.1109/LAWP.2017.2771205.

Zornoza, J. A and Encinar, J. A. Efficient phase-only synthesis of contoured-beam patterns for very large reflectarrays. *International Journal of RF and Microwave Computer-Aided Engineering*, 14, 2004. ISSN 10964290. doi: 10.1002/mmce.20028.